antioxidants

MDPI

Article

Novel NADPH Oxidase-2 Inhibitors as Potential Anti-Inflammatory and Neuroprotective Agents

Matea Juric [1,†], Varun Rawat [2,†], Radhika Amaradhi [2,‡], Jacek Zielonka [1,*] and Thota Ganesh [2,*]

[1] Department of Biophysics, Medical College of Wisconsin, Milwaukee, WI 53226, USA; mjuric@mcw.edu
[2] Department of Pharmacology and Chemical Biology, Emory University School of Medicine, Atlanta, GA 30322, USA; varun.rawat@emory.edu (V.R.); radhika.amaradhi@utsa.edu (R.A.)
* Correspondence: jzielonk@mcw.edu (J.Z.); tganesh@emory.edu (T.G.)
† These authors contributed equally to this work.
‡ Current address: Center for Innovative Drug Discovery, University of Texas San Antonio, San Antonio, TX 78249, USA.

Abstract: A family of seven NADPH oxidase enzymes (Nox1-5, Duox1-2) has been implicated in a variety of diseases, including inflammatory lung diseases, neurodegenerative diseases, cardiovascular diseases, and cancer. Here, we report the results of our studies aimed at developing novel brain-permeable Nox2 inhibitors with potential application as neuroprotective agents. Using cell-based assays, we identified a novel Nox2 inhibitor, TG15-132, that prevents PMA-stimulated oxygen consumption and reactive oxygen species (superoxide radical anion and hydrogen peroxide) formation upon acute treatment in differentiated HL60 cells. Long-term treatment with TG15-132 attenuates the induction of genes encoding Nox2 subunits, several inflammatory cytokines, and iNOS in differentiated THP-1 cells. Moreover, TG15-132 shows a relatively long plasma half-life (5.6 h) and excellent brain permeability, with a brain-to-plasma ratio (>5-fold) in rodent models. Additionally, TG15-132 does not cause any toxic effects on vital organs or blood biomarkers of toxicity in mice upon chronic dosing for seven days. We propose that TG15-132 may be used as a Nox2 inhibitor and a potential neuroprotective agent, with possible further structural modifications to increase its potency.

Keywords: NADPH oxidase; inflammation; neurodegeneration; inhibitors; neuroprotection; superoxide; hydrogen peroxide

check for updates

Citation: Juric, M.; Rawat, V.; Amaradhi, R.; Zielonka, J.; Ganesh, T. Novel NADPH Oxidase-2 Inhibitors as Potential Anti-Inflammatory and Neuroprotective Agents. *Antioxidants* **2023**, *12*, 1660. https://doi.org/10.3390/antiox12091660

Academic Editors: Michael Breitenbach and Cristina Carvalho

Received: 20 July 2023
Revised: 12 August 2023
Accepted: 18 August 2023
Published: 23 August 2023

Copyright: © 2023 by the authors. Licensee MDPI, Basel, Switzerland. This article is an open access article distributed under the terms and conditions of the Creative Commons Attribution (CC BY) license (https://creativecommons.org/licenses/by/4.0/).

1. Introduction

The production of cellular oxidizing, nitrating, and halogenating species, involving the superoxide radical anion ($O_2^{\bullet -}$), hydrogen peroxide (H_2O_2), hypochlorous acid (HOCl), peroxynitrite ($ONOO^-$), and the hydroxyl radical ($^{\bullet}OH$), collectively termed reactive oxygen species (ROS), is a common feature of pathological states involving an inflammatory component (Figure 1) [1,2]. Production of ROS by inflammatory cells is essential for the host immune response, but sustained activation of the immune system may lead to damage and dysfunction of the host cells [3]. The primary source of ROS in inflammatory cells is NADPH oxidase-2 (Nox2); therefore, the development of pharmacological approaches to inhibit Nox2 is an active area of research with significant translational potential [4,5]. Numerous rodent models of diseases with an inflammatory component showed beneficial effects following the genetic deletion of Nox2-related proteins, validating Nox2 activity as a potential therapeutic target [6–9].

Neuroinflammation, defined as an inflammatory response within the brain or spinal cord, is a critical contributing factor to many neurological diseases, ranging from status epilepticus to Alzheimer's disease, Parkinson's disease, and amyotrophic lateral sclerosis. Available data indicate a complex relationship between oxidative stress and inflammatory mediators, including both mutual activation and regulatory mechanisms [3,4,10].

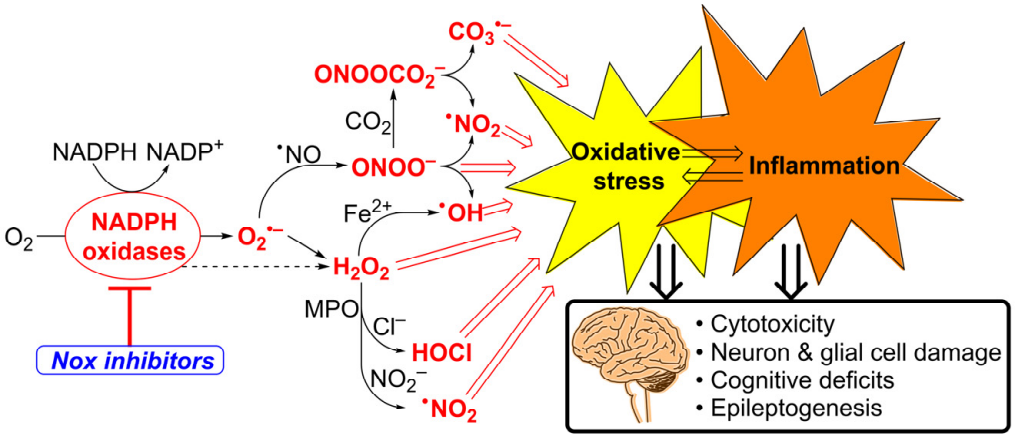


Figure 1. NOX enzymes are early inducers of ROS ($O_2^{\bullet-}$, H_2O_2), which are further converted into other, highly reactive oxidants including $^{\bullet}OH$, HOCl, $^{\bullet}NO_2$, $ONOO^-$, and $ONOO^-$-derived radicals ($^{\bullet}OH$, $^{\bullet}NO_2$, and $CO_3^{\bullet-}$), overwhelming cellular antioxidant systems and resulting in oxidative stress. Oxidative stress triggers an inflammatory cascade that can further induce ROS formation. Oxidative stress and neuroinflammation lead to the damage of neurons and other brain cells, and modify the function of glial cells, resulting in an increased risk of developing neuronal excitability and epileptogenesis.

Due to the high abundance of preclinical and clinical evidence for the involvement of oxidative and/or nitrative stress in inflammatory diseases, clinically relevant antioxidants have been proposed as possible protective agents. Both pre-clinical and clinical data provided mixed results, bringing into question the ability of oxidant scavengers to yield a therapeutic benefit [11–13]. Instead of aiming to scavenge the already formed reactive species, a more promising strategy may be to prevent their formation by blocking the activity of the enzymes responsible for the initiation of the ROS cascade (Figure 1) [14–16].

For the last two decades, there has been an active quest to identify new inhibitors of NADPH oxidases as potential therapeutic agents [17–19]. However, the results of these attempts were only moderately successful, and many putative inhibitors have been subsequently shown to act indirectly, owing to significant off-target effects on cell metabolism, or to simply interfere with the Nox2 activity assays [20–22]. One of the reasons for this has been the limited number of assays that can specifically measure the products of Nox activity: $O_2^{\bullet-}$ and H_2O_2. In fact, many assays rely on the measurement of a lesser-defined "oxidative burst," with the probes used relying on peroxidatic activity, typically accompanying increased Nox2 activity. Thus, inhibitors and substrates of peroxidases interfered with peroxidase-catalyzed probe oxidation and were disguised as apparent Nox inhibitors [21,23]. Moreover, most putative Nox inhibitors failed to show Nox-inhibitory activity in cell-free assays [20]. Recent progress in the development of redox probes and a better understanding of the chemistry behind the redox probes allowed for the design of rigorous assays to measure $O_2^{\bullet-}$ and H_2O_2 in cell-based systems, and the establishment of a high-throughput screening-compatible workflow for rigorous identification of the inhibitors of NADPH oxidases [24–26].

The application of Nox2 inhibitors for neuroprotection requires the compounds to cross the blood–brain barrier (BBB) to achieve therapeutically relevant levels in the brain. One potential strategy is to repurpose existing drugs used in neurological disorders, and several phenothiazine-based antipsychotic drugs have been shown to exhibit Nox2 inhibitory activity in vitro [25,27] and in vivo [28]. A separate approach based on medicinal chemistry-based modification of a Nox2 inhibitor of limited specificity, GSK2795039 [29], recently resulted in the development of a more specific Nox2 inhibitor, NCATS-SM7270, which shows protective effects against traumatic brain injury [30].

Here, we report the development of a novel class of BBB-permeable Nox2 inhibitors, characterize their Nox2 inhibitory potency, and determine their effects on the expression of genes associated with the inflammatory response in macrophages.

2. Materials and Methods

2.1. Materials

Coumarin-7-boronic acid (CBA) was synthesized as described previously [31], and the 0.1 M stock solution was prepared in DMSO and stored at −20 °C. Amplex Red (10-acetyl-3,7-dihydroxyphenoxazine) was purchased from Cayman Chemicals (Ann Arbor, MI, USA), and the 50 mM stock solution was prepared in DMSO and stored at −20 °C. Hydroethidine (5-ethyl-5,6-dihydro-6-phenyl-3,8-phenanthridinediamine, also known as dihydroethidium) was from Cayman Chemicals, and the 20 mM stock solution was prepared in deoxygenated DMSO, aliquoted, and stored at −80 °C. The standards for hydroethidine (HE) oxidation products were prepared as described previously [32,33]. Horseradish peroxidase (HRP, type VI) from Sigma-Aldrich (Milwaukee, WI, USA) was prepared at a concentration of 1 kU/mL in phosphate buffer (50 mM, pH 7.4) containing 100 µM DTPA and stored at 4 °C. DNA (from salmon testes) was obtained from Sigma-Aldrich and dissolved at a concentration of 2 mg/mL in Tris buffer (10 mM) containing EDTA (1 mM) and stored at 4 °C. The Cell Titer Glo 2.0 cytotoxicity assay kit was obtained from Promega (Madison, WI, USA). Phorbol 12-myristate 13-acetate (PMA) was purchased from Sigma-Aldrich, and the 10 mM stock solution was prepared in DMSO and stored at −20 °C. Diphenyleneiodonium chloride (DPI) was from Cayman Chemicals, and the 10 mM stock solution was prepared in DMSO and stored at −20 °C. Superoxide dismutase from bovine heart, catalase from *Corynebacterium glutamicum*, acetonitrile (HPLC grade), DAPP, and apocynin were obtained from Sigma-Aldrich. Diapocynin was synthesized as described previously [34]. Trifluoroacetic acid was purchased from Thermo Scientific (Waltham, MA, USA).

2.2. Cell Culture

Human promyelocytic leukemia HL60 cells (Sigma-Aldrich) were grown in RPMI 1640 medium (Gibco, 11875-093, Billings, MT, USA) supplemented with 10% FBS (Omega Scientific (Tarzana, CA, USA)), 100 units/mL penicillin, and 100 µg/mL streptomycin, and were incubated at 37 °C and 5% carbon dioxide (CO_2). For differentiation to neutrophil-like cells, HL60 cells were pelleted and resuspended in fresh media containing 1 µM of all trans-retinoic acid and incubated for four to five days. Nox2 activation was achieved by treating differentiated HL60 (*d*HL60) cells with 1 µM PMA [24]. Human leukemia monocytic cells, THP-1, were grown in RPMI 1640 medium + GlutaMAX™ (Gibco, 61870-036) and supplemented with 10% FBS, 10 mM HEPES, and 1 mM sodium pyruvate and incubated at 37 °C in 5% CO_2 environment. To induce differentiation into macrophages, THP-1 cells were treated with PMA (100 ng/mL) for 48 h. To test the efficacy of Nox2 inhibitors, treatment was performed with or without the inhibitor, along with PMA [35].

2.3. Plate Reader-Based Analyses of $O_2^{\bullet-}$ and H_2O_2 Production by Activated dHL60 Cells

Plate reader-based analyses of the production of $O_2^{\bullet-}$ and H_2O_2 by PMA-activated *d*HL60 cells were performed according to a published protocol with minor modifications [36]. Briefly, for the treatment of *d*HL60 cells with different concentrations of the compounds, 0.5 mL deep-well 96-well plates were used to dispense and store aliquots of their 10 mM DMSO solutions. Using a Multidrop™ PicoIT dispenser (Thermo Scientific), different volumes of the solutions of candidate Nox inhibitors (10 or 50 mM in DMSO) were injected into the bottom of 0.5 mL V-bottom 96-well plates; then, they were sealed with aluminum foil (VWR, Batavia, IL, USA) using a semiautomatic thermal sealer (BT LabSystems, St. Louis, MO, USA) and stored at −20 °C to reduce freeze-thawing the solutions. The plates with inhibitors were allowed to come to room temperature before the addition of the cell suspensions. *d*HL60 cells were pelleted and resuspended in HBSS (Invitrogen, Waltham, MA, USA) supplemented with 25 mM HEPES (pH 7.4) and 100 µM

DTPA to a cell density of 2×10^5 cells/mL. *d*HL60 cells were added to the V-bottom plates at a volume of 210 µL/well. Next, cells were incubated with inhibitors for 30 min at 37 °C in a CO_2-free incubator under ambient oxygen and then transferred to black, clear-bottom 96-well plates (200 µL/well) after incubation. Freshly prepared PMA plus probe solutions in HBSS (5× concentrated, 50 µL/well) included PMA (5 µM) with CBA (500 µM) or with Amplex Red (250 µM) plus HRP (0.5 U/mL) for H_2O_2 detection, or with HE (50 µM) plus DNA (0.5 mg/mL) for $O_2^{\bullet-}$ detection. Once probes + PMA were added, plates were sealed with sealing film and immediately placed in the pre-warmed plate readers (37 °C). Fluorescence intensities were monitored kinetically from the bottom of the plates every 1.3 min for a period of 2 h using Beckman Coulter (Brea, CA, USA) DTX880 and BMG Labtech (Ortenberg, Germany) FLUOstar Omega plate readers. The fluorescence excitation and emission filters used are listed in Table 1. DMSO alone and DPI (10 µM) were used as negative and positive controls, respectively. At the concentration used (10 µM), DPI did not show any cytotoxic effects, as measured by the Cell Titer Glo 2.0 cytotoxic assay, under the conditions used. The IC_{50} values were determined using at least five independent measurements, each consisting of technical quadruplicates per concentration.

Table 1. Probes and fluorescence parameters used to monitor production of $O_2^{\bullet-}$ and H_2O_2 by activated *d*HL60 cells.

Probe	Species Monitored	Excitation Filter	Emission Filter
HE [a]	$O_2^{\bullet-}$	485 nm	574 nm
HE [b]	$O_2^{\bullet-}$	370 nm	565 nm
CBA	H_2O_2	355 nm	460 nm
Amplex Red	H_2O_2	535 nm	595 nm

[a] Plate reader-based measurements. [b] Rapid HPLC analyses.

2.4. Rapid HPLC Analyses of $O_2^{\bullet-}$ Production by Activated dHL60 Cells

For high-performance liquid chromatography (HPLC)-based analyses of superoxide production by activated *d*HL60 cells, the cells (0.8 mL, 2×10^5 cells/mL) were pretreated with inhibitors for 30 min, as described above, followed by the addition of 200 µL of the mixture of PMA (5 µM) and HE (50 µM); then, they were incubated for 1 h at 37 °C in the dark. Next, 0.5 mL aliquots of the cell suspensions were transferred into 1.5 mL micro-centrifuge tubes prefilled with 10 µL of a mixture of 3,8-diamino-6-phenylphenanthridine (50 µM, used as an internal standard), superoxide dismutase, and catalase (5 mg/mL and 5 kU/mL, respectively, used to stop probe oxidation), and the tubes were centrifugated (5 min, 3000× *g*) to pellet the cells. Clear supernatants (0.2 mL) were transferred into HPLC vials and analyzed for HE, 2-hydroxyethidium (2–OH–E^+), ethidium (E^+), and diethidium (E^+–E^+) content, as described previously [37]. Briefly, an Agilent 1100 HPLC system equipped with an Ascentis Express Phenyl-Hexyl column (50 mm × 4.6 mm, 2.7 µm, Supelco, Bellefonte, PA, USA) and absorption and fluorescence detectors was used. The analytes were eluted in isocratic mode using a mobile phase consisting of 65% water, 35% acetonitrile, and 0.1% trifluoroacetic acid at a flow rate of 2 mL/min. Samples (25 µL) were injected, and the products were detected by monitoring absorbance (290 and 370 nm) and fluorescence (exc. 370 nm, emi. 565 nm) signals.

2.5. Oxygen Consumption Measurements

Oxygen consumption in *d*HL60 cells was monitored before and after the sequential addition of the candidate Nox inhibitors and PMA using a Seahorse XFe96 extracellular flux analyzer (Agilent Technologies, Santa Clara, CA, USA) [24,36]. The cell suspension was prepared in phenol red-free RPMI medium (without bicarbonate) and aliquoted (80 µL/well) into a 96-well plate to obtain a final cell number of 2×10^4 cells/well. Cells were spun down and an additional amount of RPMI medium (100 µL/well) was added gently so as not to disturb the cells at the bottom of the wells. The solutions for injections were

prepared 10× concentrated, loaded into the injection ports of the Seahorse XFe96 cartridge, and the volumes injected were 20 µL and 22.2 µL for the compounds tested and PMA, respectively. The oxygen consumption rates were monitored for 30 min before injection (baseline respiration rate), 60 min after injection of different concentrations of the candidate Nox inhibitors, and 2 h after injection of PMA (final concentration: 1 µM). Increases in OCR values after PMA injection were used as a measure of Nox2 activity.

2.6. Cytotoxicity

The cytotoxicity of the inhibitors was tested by measuring the amount of ATP in the wells containing PMA-stimulated *d*HL60 cells and the candidate inhibitors. Cells were prepared as described for the plate reader-based measurements for H_2O_2, except that the cells were maintained with the inhibitors in a CO_2-free incubator at 37 °C for 2.5 h to mirror the conditions during the fluorescence-based monitoring of H_2O_2 described above. After incubation, cells (100 µL/well) were transferred to white 96-well plates (Greiner, Kremsmünster, Austria), and the total cellular ATP amount was determined using the Cell Titer Glo 2.0 (Promega) cytotoxicity assay (100 µL/well) by measuring the luminescence intensity using a Beckman Coulter DTX880 plate reader.

2.7. Gene Expression Analysis

mRNA expression analysis was performed as previously described [38–40]. Briefly, THP-1 cells were treated with PMA (100 ng/mL) with or without the Nox2 inhibitor TG15-132 (3.0 µM) for 48 h. RNA extraction was done using the Quick-RNA miniprep kit (cat. no. R1055, Zymo Research, Irvine, CA, USA) and followed by cDNA synthesis using the qScript cDNA superMix kit (cat. no. 84035, Quantabio, Beverly, MA, USA). Quantitative real-time PCR was performed using specific primers designed to amplify target genes (Table 2). Data obtained were analyzed and converted into fold changes in expression with respect to vehicle-treated cells.

Table 2. Primers for qRT-PCR.

Gene	Accession No.	Primer Sequences
NOX2	NM_000397	F: GGTCCCATGTTTCTGTATCTC R: CCCTTCTTCTTCATCTGTAGC
p47^{phox}	NM_000265	F: GCTGGTGGGTCATCAGGAAA R: GCCCTGACTTTTGCAGGTACA
p67^{phox}	NM_000433	F: CCTGCAACTACCTTGAACCAGTT R: GGACTGCGGAGAGCTTTCC
Tnfα	NM_000594	F: CTCTTCTGCCTGCTGCACTTTG R: ATGGGCTACAGGCTTGTCACTC
IL1β	NM_000576	F: CCACAGACCTTCCAGGAGAATG R: GTGCAGTTCAGTGATCGTACAGG
β-Actin	NM_001101	F: GGTGACAGCAGTCGGTTGGAG R: AGTGGGGTGGCTTTTAGGATGG
GAPDH	NM_001256799	F: TGCACCACCAACTGCTTAGC R: GGCATGGACTGTGGTCATGAG

2.8. Plasma and Brain In Vivo Pharmacokinetics Studies

TG15-132 at a 20 mg/kg dose in a vehicle formulation of 10% DMSO, 50% PEG400, and 40% reversed osmosis-purified water (*v*/*v*) was administered to healthy male C57BL/6 mice weighing an average of 27 g by intraperitoneal (i.p.) injection. Blood samples (approximately 60 µL) were collected from the retro-orbital plexus of three animals at times 0.08, 0.25, 0.5, 1, 2, 4, 8, and 24 h after compound administration. Along with the terminal blood samples, the brain samples were also collected at the time points 0.25, 0.5, 2.0, 4.0, 8.0, and 24 h.

Blood samples were collected into labeled microtubes containing dipotassium EDTA solution (20%) as an anticoagulant. Plasma was immediately harvested from the blood by centrifugation at 4000 rpm for 10 min at 4 ± 2 °C and stored below −70 °C until bioanalysis. After isolation, brain tissue samples were rinsed three times in ice cold normal saline (for 5–10 s/rinse using ~5–10 mL normal saline in disposable petri dishes for each rinse) and dried on blotting paper. Tissue samples were homogenized using ice-cold phosphate-buffered saline (pH 7.4). The total homogenate volume (µL) was three times the tissue weight (mg). All homogenates were stored below −70 ± 10 °C until bioanalysis. Concentrations of TG15-132 in plasma and brain samples were determined by fit-for-purpose liquid chromatography with the tandem mass spectrometry method (Sai-Life, Hyderabad, India). Phoenix WinNonlin (version 8.0, Certara, Princeton, NJ, USA) was used to analyze the pharmacokinetic parameters.

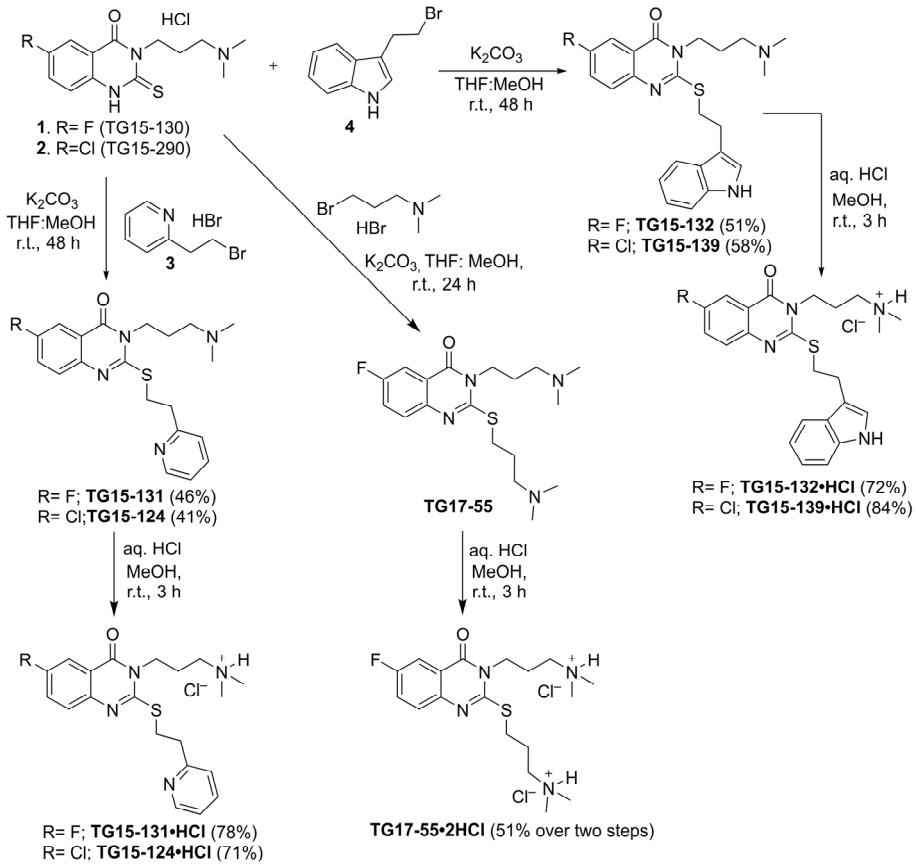
2.9. Short-Term In Vivo Toxicity

All animal experiments were performed according to protocols and guidelines approved by the Emory University Animal Care and Use Committee. The in vivo toxicity of TG15-132 was assessed using C57BL/6 mice (cat. no. 027, Charles River Laboratories, Wilmington, MA, USA). Animals were injected daily (i.p.) with saline, vehicle (DMSO 10%, PEG400 30%, water 60%), or 20 mg/kg of TG15-132 in vehicle for seven days, with body weight recorded each day. At the end of treatment, organs were harvested to study organ weight loss, and blood was collected from each mouse via cardiac puncture, and serum was isolated. Serum was analyzed for kidney function using blood urea nitrogen and creatinine, liver function using alanine amino transferase, and tissue damage using lactate dehydrogenase [41].

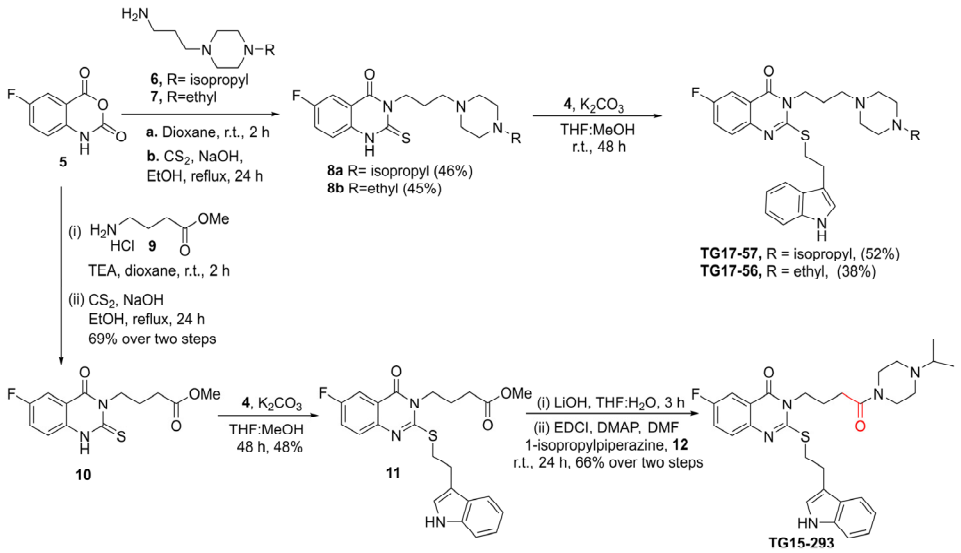
2.10. Synthesis of Nox2 Inhibitors TG15-132 and Derivatives

Previously synthesized and reported molecules, 3-(3-(dimethylamino)propyl)-2-thioxo-2,3-dihydroquinazolin-4(1H)-ones 1 and 2, were subjected to alkylation with commercially available compounds 3-(2-bromoethyl)-1H-indole (4) or 2-(2-bromorethylpyridine) (3) in the presence of potassium carbonate base to provide TG15-132, TG15-139, TG15-131, and TG15-124 in moderate yields (Scheme 1). These free bases were treated with an aqueous HCl solution to provide the corresponding hydrochloride salts. Free bases were dissolved in DMSO for the determination of the direct Nox2 inhibitory effects of the compounds, but similar effects were observed for both free bases and hydrochloride salts. In most other experiments, the hydrochloride salts of the synthesized inhibitors were used.

Similarly, four other derivatives, TG17-55, TG17-56, TG17-57, and TG15-293, were synthesized from fluoro-isatoic anhydride (5) via precursors (**8a**, **8b**, and **11**), as shown in Schemes 1 and 2. All novel compounds were characterized by nuclear magnetic resonance, liquid chromatography-mass spectrometry, and HPLC methods (Supplemental Information).



Scheme 1. Synthesis of Nox2 inhibitors. Reagents and conditions are shown in arrows, and the yields are shown in parentheses.



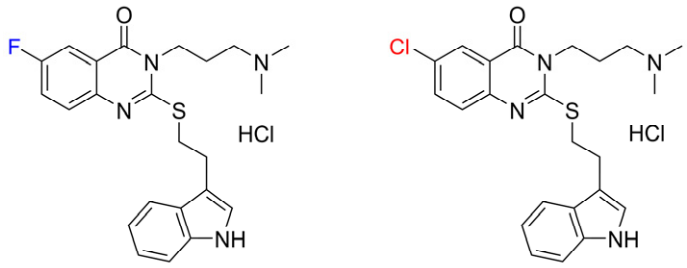
Scheme 2. Synthesis of TG15-293, TG17-56, and TG17-57 compounds. Reagents and conditions are shown in arrows, and the yields are shown in parentheses.

3. Results

3.1. Identification of Novel Nox2 Inhibitors

In an ongoing quest to identify and develop Nox2 selective inhibitors for therapeutic use, we previously conducted high-throughput screening (HTS) on a library of >200,000 compounds using a cell-free assay and found only ebselen (selenium compound)

and its sulfur congeners as modest Nox2 inhibitors [42]. Subsequently, we re-screened approximately 50 compounds from our synthetic library, including some widely used (in the literature), commercially available putative Nox2 inhibitors (DPI, apocynin, diapocynin, and others) to find genuine Nox2 selective inhibitors [24]. From these, we identified TG15-132 (Figure 2) as a genuine Nox2 inhibitor, and a few other derivatives synthesized around this compound also showed low micromolar Nox2 inhibitory activity, as detailed below.



TG15-132•HCl **TG15-139•HCl**

Figure 2. Chemical structures of the candidate Nox2 inhibitors tested. The structures of other compounds used for SAR study are shown in Schemes 1 and 2.

3.2. Characterization of Nox2 Inhibition in Differentiated HL60 Cells

We used HL60 leukemia cells differentiated with all-trans retinoic acid to neutrophil-like cells (*d*HL60) as a model to screen and characterize potential Nox2 inhibitors. Upon treatment of *d*HL60 cells with PMA, the NADPH oxidase cytosolic and membrane protein partners assemble to form a fully active complex that produces the short-lived $O_2^{\bullet -}$, which is subsequently dismutated to a more stable product, H_2O_2. Thus, monitoring the changes in H_2O_2 produced by activated *d*HL60 cells provides a convenient and high-throughput screening-compatible way to study the potency of candidate Nox2 inhibitors [24,25,36]. We used CBA to monitor H_2O_2 production, as boronate compounds react directly with H_2O_2 without the requirement of peroxidase, thus minimizing the potential interference of peroxidase substrates and inhibitors with the assay. During the reaction, CBA was converted to a blue fluorescent product, 7-hydroxycoumarin (COH, also known as umbelliferone, Figure 3A). Among the inhibitors tested, TG15-132 and TG15-139 were the most promising, with half-maximal inhibitory concentration (IC_{50}) values of 4.5 and 3.0 μM, respectively. Representative traces of CBA oxidation and titration curves for both inhibitors are shown in Figure 3B,C. To exclude the possibility that the results obtained were due to potential cytotoxicity of the tested compounds, the inhibition studies were accompanied by measurements of cell viability. As shown in Figure 3D,E, both compounds show Nox2 inhibitory potency (blue squares) at concentrations at which no decrease in cell viability (red circles) was observed.

As an orthogonal assay of H_2O_2 production, we used peroxidase-catalyzed oxidation of Amplex Red to red fluorescent resorufin (Figure 4A), one of the most widely used assays to assess extracellular H_2O_2. Consistent with the data obtained with the CBA probe, we observed dose-dependent inhibition of Amplex Red oxidation (IC_{50} = 7.9 and 5.0 μM for TG15-132 and TG15-139, respectively), confirming the ability of the compounds to block H_2O_2 production at low micromolar concentrations (Figure 4).

The IC_{50} values for all compounds showing inhibitory activity, determined using both H_2O_2 assays and the viability assay, are presented in Table 3. For comparison, we also tested DPI, a general flavoprotein inhibitor, and apocynin and its peroxidase-catalyzed oxidation product, diapocynin, in our study. Apocynin is widely used as an inhibitor of NADPH oxidase, and diapocynin was proposed to be its metabolite responsible for its inhibitory activity. However, these compounds did not show Nox2 inhibitory activity when tested at concentrations of up to 50 μM, in accordance with recent reports. DPI (10 μM) consistently showed inhibitory activity and was used in all experiments as a positive control.

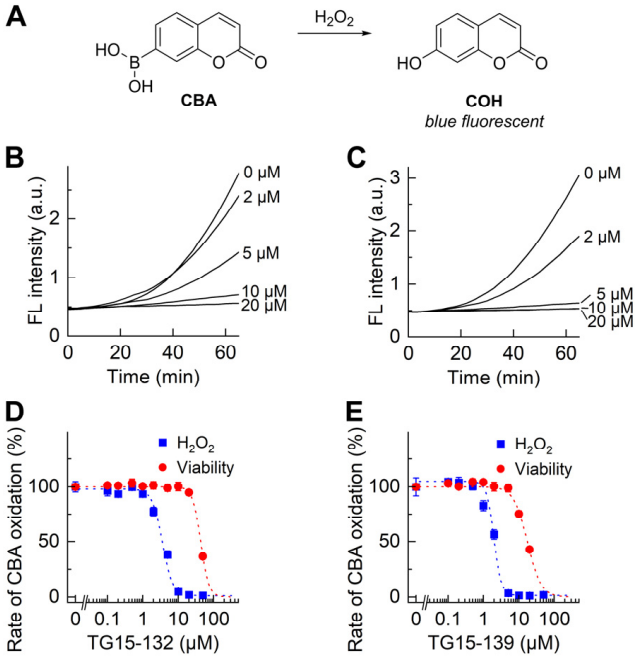


Figure 3. Inhibition of H_2O_2 production by activated *d*HL60 cells by selected inhibitors, as measured using a CBA probe. (**A**) Chemical principle of H_2O_2 measurement. (**B**,**C**) Kinetic traces of probe oxidation in the absence and presence of the inhibitors tested. (**D**,**E**) Concentration dependence of the inhibitory effects of TG15-132 (**D**) and TG15-139 (**E**) candidate inhibitors on H_2O_2 production (blue symbols) and cell viability (red symbols). Dashed lines represent fitted curves used to determine the IC_{50} values.

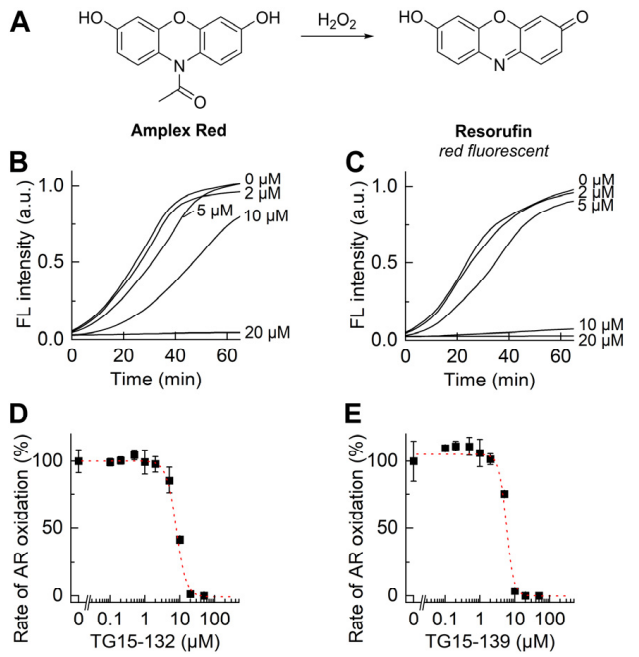


Figure 4. Inhibition of H_2O_2 production by activated *d*HL60 cells by selected inhibitors, as measured using an Amplex Red-based assay. (**A**) Chemical principle of H_2O_2 measurement. (**B**,**C**) Kinetic traces of probe oxidation in the absence and presence of the inhibitors tested. (**D**,**E**) Concentration dependence of the inhibitory effects of TG15-132 (**D**) and TG15-139 (**E**) candidate inhibitors on H_2O_2 production. Dashed lines represent fitted curves used to determine the IC_{50} values.

Table 3. Determined IC_{50} values for the inhibition of H_2O_2 production by activated *d*HL60 cells and for cell viability.

Compound	CBA Assay	Amplex Red Assay	Viability Assay [a]
TG15-132	4.3 ± 1.3 [b]	7.9 ± 3.0 [b]	34.5 ± 6.0
TG15-139	3.1 ± 1.4 [b]	4.9 ± 2.3 [b]	14.1 ± 1.7
TG15-293	23.6 ± 18.1	67.8 ± 2.6	38.3 ± 7.5
TG17-56	5.3 ± 0.6	7.8 ± 4.0	16.7 ± 2.5
TG17-57	7.0 ± 2.8	9.2 ± 0.4	20.7 ± 5.0

[a] Cell Titer Glo 2.0 cytotoxic assay; [b] $n \geq 8$ (number of independent determinations).

3.3. Structure–Activity Relationship Studies

After conducting a limited number of structure–activity relationship studies on this class of compounds, we observed that replacing the indole moiety (connected to sulfur with an ethylene linker [TG15-132 and TG15-139]) with a pyridine moiety (see TG15-131 and TG15-124 in Scheme 1) resulted in a significant loss in Nox2 inhibitory potency (not shown). Likewise, replacing the same indole-moiety with a much simpler amino-alkyl chain (TG17-55, Scheme 1) also eliminated potency. We then wondered whether keeping the indole moiety intact while modifying the N,N-dimethylaminopropyl moiety (other region) would retain the potency. To answer this question, we synthesized two compounds, TG17-56 and TG17-57, as shown in Scheme 2. Interestingly, these derivatives showed low micromolar potencies (5.3 μM and 7 μM, Table 3), suggesting that this region is amenable for structural modification. Furthermore, we have also synthesized a derivative, TG15-293, which bears an extra carbonyl group in the structure in comparison to TG17-57. This compound showed about 3-fold less potency than TG17-57 in the CBA assay and about 7-fold less potency in the Amplex Red assay (Table 3). Future studies will expand this region further, and the core quinazoline for structural modification.

Comparison of the H_2O_2 production inhibitory potency and cell cytotoxicity of the tested candidate inhibitors led to the selection of the TG15-132 compound as the lead hit, showing high potency and low cytotoxicity. This compound was, therefore, advanced for additional confirmatory assays, including the measurements of the effect of TG15-132 on PMA-stimulated $O_2^{\bullet-}$ production and O_2 consumption by *d*HL60 cells.

We used hydroethidine (HE) to monitor $O_2^{\bullet-}$ production. In the presence of $O_2^{\bullet-}$, HE is converted to a $O_2^{\bullet-}$-specific red fluorescent product, 2–OH–E^+ (Figure 5A), while other oxidants may form another fluorescent product, E^+, and dimeric products, including E^+–E^+ [43,44]. The fluorescence intensity of 2–OH–E^+ and E^+ can be further increased by binding to DNA; thus, the assay medium was supplemented with DNA for plate reader-based monitoring of probe oxidation. Stimulation of *d*HL60 cells with PMA led to a time-dependent increase in the fluorescence intensity, which was dose-dependently inhibited by cell pretreatment with TG15-132 (Figure 5B,C). To test whether the fluorescence signal was due to superoxide-dependent probe oxidation, the plate reader-based analyses were accompanied by rapid HPLC analysis of the assay media after 1 h of incubation. Oxidation of HE was accompanied by the formation of 2–OH–E^+ as the major product, and both the extent of HE consumption and 2–OH–E^+ formation were inhibited by cell pretreatment with TG15-132 in a dose-dependent manner (Figure 5D,E). This confirms that the compound blocks $O_2^{\bullet-}$ production by activated *d*HL60 cells.

Further confirmation of the Nox2 inhibitory activity of TG15-132 was obtained by measuring the rates of PMA-stimulated oxygen consumption. We used the Seahorse XFe96 Extracellular Flux Analyzer, which enables repeated measurements of oxygen consumption rates and sequential injections of up to four different treatments during measurements, eliminating the need for chemical probes. As shown in Figure 6, the injection of PMA resulted in an immediate increase in the oxygen consumption rate, which represents the oxidative burst due to Nox2 activation. The injection of candidate inhibitors prior to PMA

injection enabled monitoring of Nox2 inhibitory activity as well as potential mitochondrial-inhibitory activity. Upon establishment of the stable baseline, the compound was injected, and oxygen consumption rates were monitored for 1 h before activation of Nox2 by PMA. There was no inhibition of basal respiration at concentrations at which the compound showed significant inhibition of PMA-induced OCR. This further confirms that TG15-132 inhibits Nox2 activity in PMA-stimulated *d*HL60 cells without affecting mitochondrial function and viability.

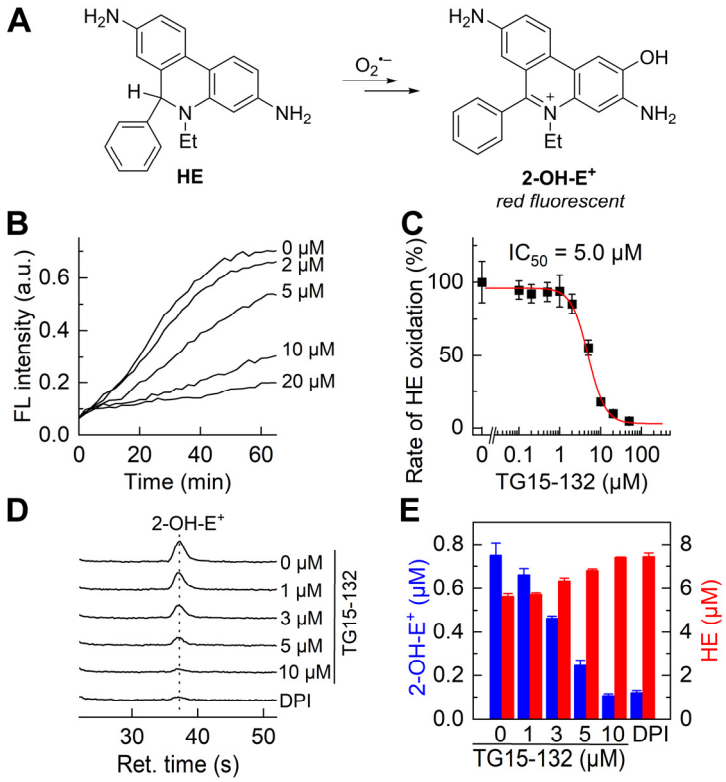


Figure 5. Inhibition of $O_2^{\bullet-}$ production by activated *d*HL60 cells by TG15-132, as measured using hydroethidine-based assays. (**A**) Chemical principle of $O_2^{\bullet-}$ measurement. (**B**) Kinetic traces of probe oxidation in the absence and presence of different concentrations of TG15-132. (**C**) Concentration dependence of the inhibitory effects of TG15-132 on $O_2^{\bullet-}$ production. Red line represents the fitted curve used to determine the IC_{50} value. (**D**) HPLC chromatograms of 2–OH–E^+ formed at different concentrations of TG15-132 or 10 µM DPI. (**E**) Quantitative analyses of the HPLC data on the levels of 2–OH–E^+ formed (blue bars) and HE probe (red bars) consumption at different concentrations of TG15-132.

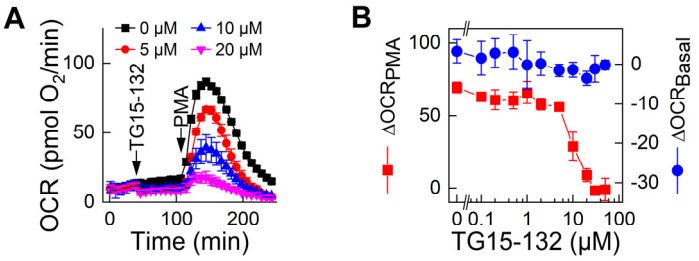


Figure 6. Inhibition of oxygen consumption by activated *d*HL60 cells by TG15-132, as measured using Seahorse XFe96-based respirometry. (**A**) Kinetic traces of OCR before and after sequential injection of TG15-132 and PMA. (**B**) Concentration dependence of the inhibitory effects of TG15-132 on basal (blue circles) and PMA-stimulated (red squares) OCR.

3.4. Effect of TG15-132 on Molecular Markers of Inflammation in THP-1 Cells

The relationship between redox stress and inflammation involves cytokine-dependent activation of pro-inflammatory genes and increased expression of NADPH oxidase components. Previous reports suggest that putative NADPH oxidase inhibitors may also inhibit the protein expression of NADPH oxidase components, which may contribute to the effects observed [45,46]. While the data obtained using *d*HL60 cells (described above) involved acute treatment and inhibition of Nox2 activity, we used human THP-1 cells differentiated to express a macrophage phenotype to study the effect of the selected Nox2 inhibitor, TG15-132, on the expression of Nox2 components and other proinflammatory genes. THP-1 cells were treated with PMA (100 ng/mL) for 48 h, with or without TG15-132 (3 μM), followed by mRNA extraction and analysis of gene expression. Treatment with PMA led to increased expression of *gp91^{phox}*, *p47^{phox}*, *p67^{phox}*, and *IL-1β*, whereas expression of *TNF* was significantly reduced (Figure 7A). TG15-132 treatment reduced the expression of *gp91^{phox}*, *p47^{phox}*, *p67^{phox}*, *IL-1β*, and *TNF* compared with cells treated with PMA alone. In an additional experiment, TG15-132 was evaluated against the effects of GSK 2795039, a recently reported Nox2 inhibitor (Figure 7B). Under the same experimental conditions, TG15-132 treatment led to a statistically significant reduction in the expression of *p47^{phox}*, *IL-1β*, and *TNF*, whereas treatment with GSK 2795039 (3 μM) did not reduce the expression of Nox2 components and inflammatory mediators, and the expression of *TNF* was increased compared with PMA-treated cells.

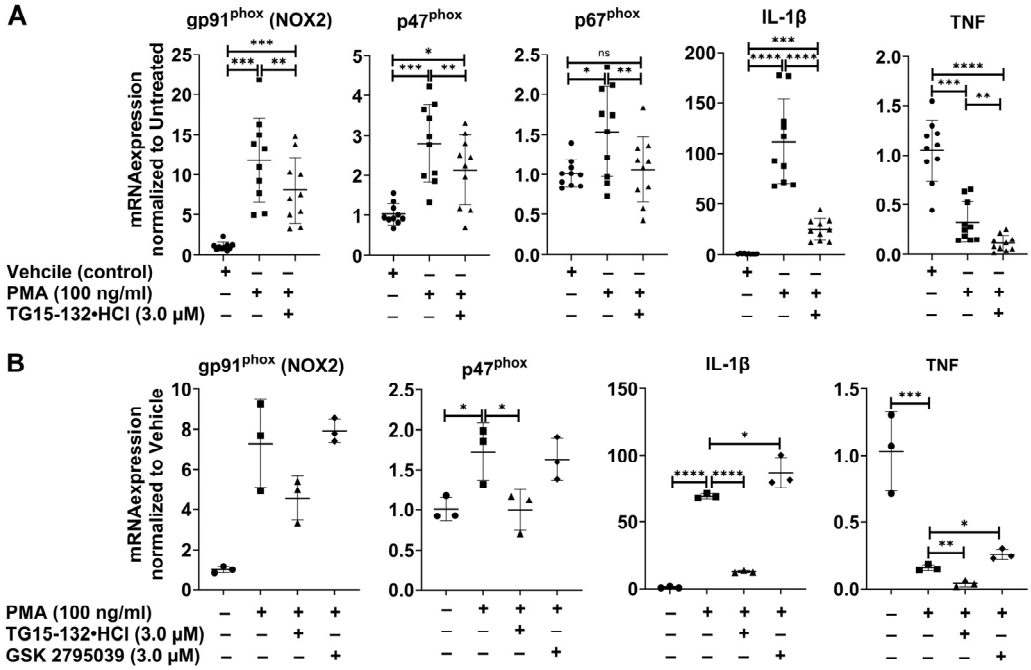


Figure 7. (**A**) Nox2 inhibitor TG15-132 suppresses the induction of Nox2 and inflammatory mediators in human THP-1 cells. (**B**) Nox2 inhibitor TG15-132 (3 μM) performed significantly better compared with GSK 2795039 (3 μM) in alleviating the effect of PMA treatment in THP-1 cells. THP-1 cells were treated with PMA with or without TG15-132 or a known Nox2 inhibitor, GSK 2795039, for 48 h, followed by the analysis of the mRNA expression levels. A one-way ANOVA with Tukey's multiple comparison test was used for analysis. * $p < 0.05$, ** $p < 0.01$, *** $p < 0.001$, **** $p < 0.0001$, ns—not significant ($p > 0.05$).

3.5. In Vivo Pharmacokinetic and Toxicity Study of Seven Day Dosing

Rapid metabolism and the inability to cross the BBB represent major obstacles in the application of bioactive agents in neurodegenerative diseases. Based on the premise that Nox2 plays a major role in oxidative damage and exacerbates neurodegenerative dis-

eases, we envision applications of brain-permeable Nox2 inhibitors in mechanistic studies in vivo, and, long-term, in the development of novel therapeutic strategies. Therefore, we performed in vivo pharmacokinetics studies to determine the time profile of plasma concentration and accumulation of TG15-132 in the brain tissue of Sprague Dawley rats and C57BL6 mice. As shown in Figure 8, TG15-132 displayed a plasma half-life of 3.7 h and a brain half-life of 5.6 h after a single dose of 20 mg/kg by i.p. injection in Sprague Dawley rats, with an AUCinf of 10,180 (h·ng/mL) and clearance rate of 32.8 (mL/min/kg). Interestingly, the brain-to-plasma ratio for this compound is exceptionally high (>10-fold up to 8 h after administration in Sprague Dawley rats) (n = 2 technical and n = 2 experimental repeats). Similarly, C57BL6 mice that were administered a single dose of 20 mg/kg TG15-132 (i.p. injection) displayed a plasma half-life and brain half-life of 2.7 h, with a brain-to-plasma ratio >6-fold, indicating that TG15-132 is a highly suitable compound for proof-of-concept studies and a novel chemical scaffold useful for optimizing and enhancing the potency of this class of Nox2 inhibitors. Likewise, TG15-139 displayed exceptionally high brain-penetration with a brain-to-plasma ratio >23-fold (not shown), suggesting that high brain penetration is not restricted to a single compound in this class.

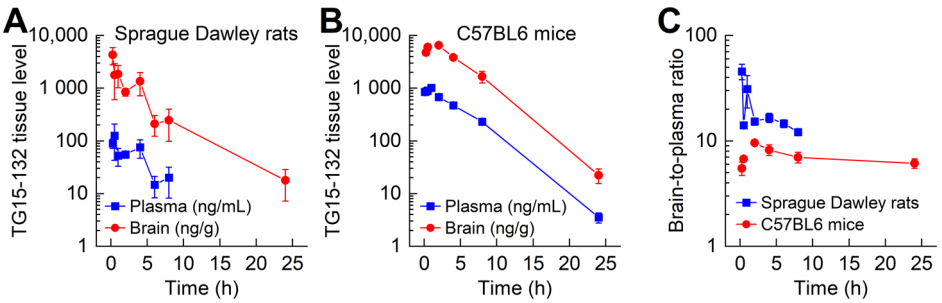


Figure 8. Plasma and brain levels of TG15-132 in male Sprague Dawley rats (**A**) and male C57BL6 mice (**B**) after single i.p. administration of TG15-132 solution (20 mg/kg b.w.). (**C**) Brain-to-plasma ratio values.

We found the pharmacokinetics of these compounds to be impressive, so we wanted to determine whether TG15-132 would show any in vivo toxicity to the animals before we advanced to potential proof-of-concept studies in preclinical animal disease models. Considering the observed pharmacokinetic profile and efficient accumulation of TG15-132 in the brain (Figure 8), we envisioned that a week-long treatment may be sufficient to result in inhibition of both Nox2 activity and inhibition of the expression of inflammatory markers. Therefore, we selected a seven-day administration period to determine the potential toxicity of TG15-132. As shown in Figure 9, seven days of daily administration of TG15-132 (20 mg/kg) caused only a marginal and nonsignificant loss of body weight (7%), and no changes to the weights of the lung, liver, or brain. We also analyzed the serum to look for kidney, lung, and tissue injury markers. We observed no differences between mice treated with vehicle vs. TG15-132 (n = 6). TG15-132 treatment led to a significant drop in blood urea nitrogen compared with saline-treated mice.

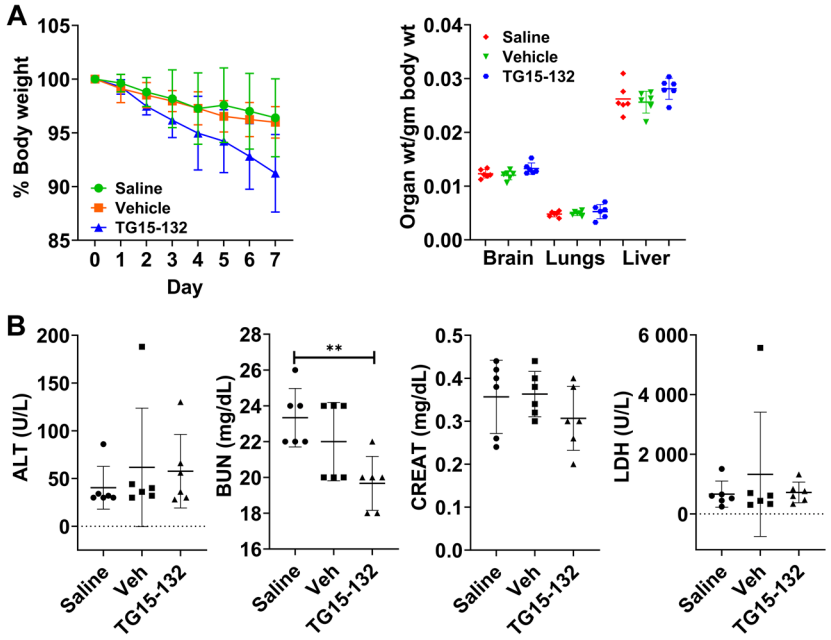


Figure 9. Potential in vivo toxicity of TG15-132. (**A**) Body weight over the course of the mice ($n = 6$) treatment with vehicle or TG15-132 (i.p., 20 mg/kg; vehicle: DMSO 10%, PEG400 30%, water 60%). Two-way ANOVA with Tukey's multiple comparison test was used for analysis. (**B**) Nox2 inhibitor TG15-132•HCl (20 mg/kg) did not lead to a negative effect on liver or kidney function or to tissue damage. Animals treated with saline, vehicle, or TG15-132•HCl (20 mg/kg) were sacrificed, blood was collected with cardiac puncture, and serum was isolated. Serum was analyzed for kidney function using blood urea nitrogen (BUN) and creatinine (CREAT), liver function using alanine amino transferase (ALT), and tissue damage using lactate dehydrogenase (LDH). One-way ANOVA with Tukey's multiple comparison test was used for analysis. ** $p < 0.01$.

4. Discussion

The key findings presented in this manuscript include the identification of a novel and relatively potent Nox2 inhibitor with an IC_{50} at low micromolar concentrations and favorable cytotoxic and in vivo safety characteristics. The presented data provide a foundation for a class of Nox2 inhibitors that can be used as basic chemical scaffolds to develop future, more potent Nox2 inhibitor candidates. The described compounds exhibit potency in the low micromolar range, which is multifold lower than the widely used experimental NADPH oxidase inhibitor apocynin. The determined inhibitory potency in the low micromolar region may enable targeting of various diseases that have shown involvement of NADPH oxidase dysregulation as either a core cause or a secondary effect in the pathogenesis. Significant efforts are needed to optimize and improve upon our discoveries to develop potential candidate compounds that are more potent and have better properties.

Oxidative stress has been associated with the initiation and progression of various neurological disorders [47–49]. Furthermore, oxidative stress is linked to alterations in the inflammatory response in models of these diseases [47,50–52]. Therefore, studying the relationship between NADPH oxidase inhibition and the alteration of inflammatory mediators in response to treatment with NADPH oxidase inhibitors is key for a thorough understanding of the mechanism(s) of action of the inhibitors. Not only did we observe inhibition of Nox2 activity and a significant reduction in the expression of key subunits of the NADPH oxidase complex with the developed inhibitor (TG15-132), we also observed a reduction in the levels of inflammatory markers in the cell model used. Therefore, this new class of Nox2 inhibitors is promising for applications where inhibition of markers of oxidative stress and inflammation is desired, and for the development of novel drug candidates targeting NADPH oxidase and inflammation in diseases.

When it comes to targeting neurological disorders, the main roadblock faced by any potential candidate is permeability across the BBB to reach the central nervous system. TG15-132 shows very promising permeability across the BBB, with a brain-to-plasma ratio staying above the 10-fold mark for at least 8 h post injection. This observation further supports TG15-132 as a potential candidate for targeting NADPH oxidase in vivo in models of neurodegenerative diseases.

Although the described Nox2 inhibitor candidate shows significantly better characteristics compared with many currently available Nox2 inhibitors, its use as a selective Nox2 inhibitor and mechanistic tool requires further research, including models for other NADPH oxidase isoforms and cell-free Nox2 assays to decipher the mechanism of inhibition. The presented data suggest that both direct interaction of TG15-132 with NADPH oxidase subunits and transcriptional regulation of the expression of Nox2 subunits may be involved. It seems unlikely that transcriptional regulation is responsible for the inhibitory activity observed in *d*HL60 cells, as preincubation with the inhibitors in all the activity assays lasted 30 min, while the effects on the expression of the transcripts of NADPH oxidase-2 subunits were observed after 48-h incubation. Whether there is a direct link between these two activities remains to be established. In addition, while we presented initial structure-activity relationship data that show the motifs responsible/required for the inhibitory activity observed, rigorous structural modification studies are needed to optimize the structure of candidates with optimal physical and functional characteristics. Furthermore, before application of the identified inhibitor for neuroprotection, additional testing of its effect on the function of microglial and neuronal cells is needed to extend the observed Nox2 inhibitory activity and low cytotoxicity to brain-specific cell types.

In summary, TG15-132 and related compounds are a promising class of bioactive compounds that are candidates for targeting NADPH oxidase in models of neurodegenerative diseases. TG15-132 shows a Nox2 inhibitory potency superior to numerous less potent and nonspecific inhibitors currently being used (e.g., apocynin). Furthermore, TG15-132 has the ability to modulate the transcription of NADPH oxidase subunits gp91^{phox}, p47^{phox}, and p67^{phox}, as well as inflammatory mediators, including IL-1β. Finally, TG15-132 shows highly desirable BBB permeability, with an exceptional brain-to-plasma ratio and significantly longer retention in the brain. Collectively, all of the features of TG15-132 point to it being a highly promising therapeutic agent to target neurological diseases where their etiology and/or pathogenesis is directly or indirectly related to NADPH oxidase dysregulation.

5. Conclusions

The need for reliable Nox2 inhibitors for biomedical research compelled us to develop a distinct class of Nox-selective inhibitors. In this study, we report a novel quinazoline class of compounds as Nox2 inhibitors. These compounds display low micromolar potency, high brain penetration, and anti-inflammatory properties in cellular models in vitro, and may be suitable compounds for preclinical studies using in vitro and in vivo disease models.

Supplementary Materials: The following supporting information can be downloaded at: https://www.mdpi.com/article/10.3390/antiox12091660/s1, (i) General analytical procedure, (ii) Synthesis of the compounds, and (iii) ^{1}H NMR, ^{19}F NMR, MS spectra and HPLC chromatograms of compounds.

Author Contributions: Conceptualization, T.G. and J.Z.; methodology, J.Z. and T.G.; validation, M.J., V.R., J.Z. and T.G.; formal analysis, M.J., V.R. and J.Z.; investigation, M.J., V.R., R.A. and J.Z.; resources, T.G. and J.Z.; data curation, T.G. and J.Z.; writing—original draft preparation, J.Z. and T.G.; writing—review and editing, M.J., V.R., R.A., J.Z. and T.G.; visualization, J.Z. and V.R.; supervision, J.Z. and T.G.; project administration, J.Z. and T.G.; funding acquisition, J.Z. and T.G. All authors have read and agreed to the published version of the manuscript.

Funding: This work was supported by NIH/NIA grant U01 AG052460 (T.G.). The liquid handling equipment used to monitor the Nox2 inhibitory activity of the compounds tested was purchased using funds from the Advancing a Healthier Wisconsin Endowment (project 5520583: Small Volume Multi-well Plate Dispensers for Screening Drug Combinations) awarded to J.Z.

Institutional Review Board Statement: Experimental procedures were performed in accordance with the National Institutes of Health Guide for the Care and Use of Laboratory Animals. The animal study protocol (PROTO201700775) was reviewed and approved on 07/05/2019 by the Institutional Animal Care and Use Committee of Emory University.

Informed Consent Statement: Not applicable.

Data Availability Statement: The data presented in this study are available in the figures and tables included within the manuscript and the Supplementary Data.

Acknowledgments: J.Z. thanks B. Kalyanaraman (Medical College of Wisconsin) for providing access to the plate readers and HPLC instruments for the completion of this study.

Conflicts of Interest: T.G., J.Z. and R.A. are inventors of patent application Quinazoline derivatives, pharmaceutical compositions, and therapeutic uses related to Nox inhibition (WO2022225866A1).

References

1. Forrester, S.J.; Kikuchi, D.S.; Hernandes, M.S.; Xu, Q.; Griendling, K.K. Reactive Oxygen Species in Metabolic and Inflammatory Signaling. *Circ. Res.* **2018**, *122*, 877–902. [CrossRef] [PubMed]
2. Hoffmann, M.H.; Griffiths, H.R. The dual role of Reactive Oxygen Species in autoimmune and inflammatory diseases: Evidence from preclinical models. *Free Radic. Biol. Med.* **2018**, *125*, 62–71. [CrossRef] [PubMed]
3. Nocella, C.; D'Amico, A.; Cammisotto, V.; Bartimoccia, S.; Castellani, V.; Loffredo, L.; Marini, L.; Ferrara, G.; Testa, M.; Motta, G.; et al. Structure, Activation, and Regulation of NOX2: At the Crossroad between the Innate Immunity and Oxidative Stress-Mediated Pathologies. *Antioxidants* **2023**, *12*, 429. [CrossRef] [PubMed]
4. Hou, L.; Zhang, L.; Hong, J.S.; Zhang, D.; Zhao, J.; Wang, Q. Nicotinamide Adenine Dinucleotide Phosphate Oxidase and Neurodegenerative Diseases: Mechanisms and Therapy. *Antioxid. Redox Signal.* **2020**, *33*, 374–393. [CrossRef]
5. Bonner, M.Y.; Arbiser, J.L. Targeting NADPH oxidases for the treatment of cancer and inflammation. *Cell. Mol. Life Sci.* **2012**, *69*, 2435–2442. [CrossRef] [PubMed]
6. Hernández-Espinosa, D.R.; Massieu, L.; Montiel, T.; Morán, J. Role of NADPH oxidase-2 in the progression of the inflammatory response secondary to striatum excitotoxic damage. *J. Neuroinflamm.* **2019**, *16*, 91. [CrossRef]
7. Hu, C.-F.; Wu, S.-P.; Lin, G.-J.; Shieh, C.-C.; Hsu, C.-S.; Chen, J.-W.; Chen, S.-H.; Hong, J.-S.; Chen, S.-J. Microglial Nox2 Plays a Key Role in the Pathogenesis of Experimental Autoimmune Encephalomyelitis. *Front. Immunol.* **2021**, *12*, 638381. [CrossRef]
8. Khayrullina, G.; Bermudez, S.; Hopkins, D.; Yauger, Y.; Byrnes, K.R. Differential effects of NOX2 and NOX4 inhibition after rodent spinal cord injury. *PLoS ONE* **2023**, *18*, e0281045. [CrossRef]
9. Huang, W.-Y.; Liu, K.-H.; Lin, S.; Chen, T.-Y.; Tseng, C.-Y.; Chen, H.-Y.; Wu, H.-M.; Hsu, K.-S. NADPH oxidase 2 as a potential therapeutic target for protection against cognitive deficits following systemic inflammation in mice. *Brain Behav. Immun.* **2020**, *84*, 242–252. [CrossRef]
10. Singel, K.L.; Segal, B.H. NOX2-dependent regulation of inflammation. *Clin. Sci.* **2016**, *130*, 479–490. [CrossRef]
11. Steinhubl, S.R. Why have antioxidants failed in clinical trials? *Am. J. Cardiol.* **2008**, *101*, 14d–19d. [CrossRef] [PubMed]
12. van der Pol, A.; van Gilst, W.H.; Voors, A.A.; van der Meer, P. Treating oxidative stress in heart failure: Past, present and future. *Eur. J. Heart Fail.* **2019**, *21*, 425–435. [CrossRef] [PubMed]
13. Schmidt, H.H.; Stocker, R.; Vollbracht, C.; Paulsen, G.; Riley, D.; Daiber, A.; Cuadrado, A. Antioxidants in Translational Medicine. *Antioxid. Redox Signal.* **2015**, *23*, 1130–1143. [CrossRef] [PubMed]
14. Sassetti, E.; Clausen, M.H.; Laraia, L. Small-Molecule Inhibitors of Reactive Oxygen Species Production. *J. Med. Chem.* **2021**, *64*, 5252–5275. [CrossRef] [PubMed]
15. Diebold, B.A.; Smith, S.M.; Li, Y.; Lambeth, J.D. NOX2 As a Target for Drug Development: Indications, Possible Complications, and Progress. *Antioxid. Redox Signal.* **2015**, *23*, 375–405. [CrossRef]
16. Eastman, C.L.; D'Ambrosio, R.; Ganesh, T. Modulating neuroinflammation and oxidative stress to prevent epilepsy and improve outcomes after traumatic brain injury. *Neuropharmacology* **2020**, *172*, 107907. [CrossRef]
17. Cifuentes-Pagano, E.; Meijles, D.N.; Pagano, P.J. The quest for selective Nox inhibitors and therapeutics: Challenges, triumphs and pitfalls. *Antioxid. Redox Signal.* **2014**, *20*, 2741–2754. [CrossRef]
18. Cifuentes-Pagano, E.; Csanyi, G.; Pagano, P.J. NADPH oxidase inhibitors: A decade of discovery from Nox2ds to HTS. *Cell. Mol. Life Sci.* **2012**, *69*, 2315–2325. [CrossRef]
19. Altenhofer, S.; Radermacher, K.A.; Kleikers, P.W.; Wingler, K.; Schmidt, H.H. Evolution of NADPH Oxidase Inhibitors: Selectivity and Mechanisms for Target Engagement. *Antioxid. Redox Signal.* **2015**, *23*, 406–427. [CrossRef]

20. Augsburger, F.; Filippova, A.; Rasti, D.; Seredenina, T.; Lam, M.; Maghzal, G.; Mahiout, Z.; Jansen-Dürr, P.; Knaus, U.G.; Doroshow, J.; et al. Pharmacological characterization of the seven human NOX isoforms and their inhibitors. *Redox Biol.* **2019**, *26*, 101272. [CrossRef]
21. Reis, J.; Massari, M.; Marchese, S.; Ceccon, M.; Aalbers, F.S.; Corana, F.; Valente, S.; Mai, A.; Magnani, F.; Mattevi, A. A closer look into NADPH oxidase inhibitors: Validation and insight into their mechanism of action. *Redox Biol.* **2020**, *32*, 101466. [CrossRef] [PubMed]
22. Wind, S.; Beuerlein, K.; Eucker, T.; Muller, H.; Scheurer, P.; Armitage, M.E.; Ho, H.; Schmidt, H.H.; Wingler, K. Comparative pharmacology of chemically distinct NADPH oxidase inhibitors. *Br. J. Pharmacol.* **2010**, *161*, 885–898. [CrossRef] [PubMed]
23. Li, Y.; Ganesh, T.; Diebold, B.A.; Zhu, Y.; McCoy, J.W.; Smith, S.M.; Sun, A.; Lambeth, J.D. Thioxo-dihydroquinazolin-one Compounds as Novel Inhibitors of Myeloperoxidase. *ACS Med. Chem. Lett.* **2015**, *6*, 1047–1052. [CrossRef] [PubMed]
24. Zielonka, J.; Cheng, G.; Zielonka, M.; Ganesh, T.; Sun, A.; Joseph, J.; Michalski, R.; O'Brien, W.J.; Lambeth, J.D.; Kalyanaraman, B. High-throughput assays for superoxide and hydrogen peroxide: Design of a screening workflow to identify inhibitors of NADPH oxidases. *J. Biol. Chem.* **2014**, *289*, 16176–16189. [CrossRef]
25. Zielonka, J.; Zielonka, M.; VerPlank, L.; Cheng, G.; Hardy, M.; Ouari, O.; Ayhan, M.M.; Podsiadly, R.; Sikora, A.; Lambeth, J.D.; et al. Mitigation of NADPH Oxidase 2 Activity as a Strategy to Inhibit Peroxynitrite Formation. *J. Biol. Chem.* **2016**, *291*, 7029–7044. [CrossRef]
26. Zielonka, J.; Hardy, M.; Michalski, R.; Sikora, A.; Zielonka, M.; Cheng, G.; Ouari, O.; Podsiadły, R.; Kalyanaraman, B. Recent Developments in the Probes and Assays for Measurement of the Activity of NADPH Oxidases. *Cell Biochem. Biophys.* **2017**, *75*, 335–349. [CrossRef]
27. Seredenina, T.; Chiriano, G.; Filippova, A.; Nayernia, Z.; Mahiout, Z.; Fioraso-Cartier, L.; Plastre, O.; Scapozza, L.; Krause, K.H.; Jaquet, V. A subset of N-substituted phenothiazines inhibits NADPH oxidases. *Free Radic. Biol. Med.* **2015**, *86*, 239–249. [CrossRef]
28. Seredenina, T.; Nayernia, Z.; Sorce, S.; Maghzal, G.J.; Filippova, A.; Ling, S.C.; Basset, O.; Plastre, O.; Daali, Y.; Rushing, E.J.; et al. Evaluation of NADPH oxidases as drug targets in a mouse model of familial amyotrophic lateral sclerosis. *Free Radic. Biol. Med.* **2016**, *97*, 95–108. [CrossRef]
29. Hirano, K.; Chen, W.S.; Chueng, A.L.; Dunne, A.A.; Seredenina, T.; Filippova, A.; Ramachandran, S.; Bridges, A.; Chaudry, L.; Pettman, G.; et al. Discovery of GSK2795039, a Novel Small Molecule NADPH Oxidase 2 Inhibitor. *Antioxid. Redox Signal.* **2015**, *23*, 358–374. [CrossRef]
30. Mason, H.; Rai, G.; Kozyr, A.; De Jonge, N.; Gliniewicz, E.; Berg, L.J.; Wald, G.; Dorrier, C.; Henderson, M.J.; Zakharov, A.; et al. Development of an improved and specific inhibitor of NADPH oxidase 2 to treat traumatic brain injury. *Redox Biol.* **2023**, *60*, 102611. [CrossRef]
31. Zielonka, J.; Sikora, A.; Joseph, J.; Kalyanaraman, B. Peroxynitrite is the major species formed from different flux ratios of co-generated nitric oxide and superoxide: Direct reaction with boronate-based fluorescent probe. *J. Biol. Chem.* **2010**, *285*, 14210–14216. [CrossRef]
32. Zielonka, J.; Vasquez-Vivar, J.; Kalyanaraman, B. Detection of 2-hydroxyethidium in cellular systems: A unique marker product of superoxide and hydroethidine. *Nat. Protoc.* **2008**, *3*, 8–21. [CrossRef]
33. Zielonka, J.; Hardy, M.; Kalyanaraman, B. HPLC study of oxidation products of hydroethidine in chemical and biological systems: Ramifications in superoxide measurements. *Free Radic. Biol. Med.* **2009**, *46*, 329–338. [CrossRef] [PubMed]
34. Dranka, B.P.; Gifford, A.; Ghosh, A.; Zielonka, J.; Joseph, J.; Kanthasamy, A.G.; Kalyanaraman, B. Diapocynin prevents early Parkinson's disease symptoms in the leucine-rich repeat kinase 2 (LRRK2R^{1441}G) transgenic mouse. *Neurosci. Lett.* **2013**, *549*, 57–62. [CrossRef] [PubMed]
35. Edwards, E.E.; Thomas, S.N. P-Selectin and ICAM-1 synergy in mediating THP-1 monocyte adhesion in hemodynamic flow is length dependent. *Integr. Biol.* **2017**, *9*, 313–327. [CrossRef] [PubMed]
36. Zielonka, J.; Zielonka, M.; Cheng, G.; Hardy, M.; Kalyanaraman, B. High-Throughput Screening of NOX Inhibitors. *Methods Mol. Biol.* **2019**, *1982*, 429–446. [CrossRef]
37. Zielonka, J.; Zielonka, M.; Kalyanaraman, B. HPLC-Based Monitoring of Oxidation of Hydroethidine for the Detection of NADPH Oxidase-Derived Superoxide Radical Anion. *Methods Mol. Biol.* **2019**, *1982*, 243–258. [CrossRef]
38. Rawat, V.; Eastman, C.L.; Amaradhi, R.; Banik, A.; Fender, J.S.; Dingledine, R.J.; D'Ambrosio, R.; Ganesh, T. Temporal Expression of Neuroinflammatory and Oxidative Stress Markers and Prostaglandin E2 Receptor EP2 Antagonist Effect in a Rat Model of Epileptogenesis. *ACS Pharmacol. Transl. Sci.* **2023**, *6*, 128–138. [CrossRef]
39. Rawat, V.; Goux, W.; Piechaczyk, M.; SR, D.M. c-Fos Protects Neurons Through a Noncanonical Mechanism Involving HDAC3 Interaction: Identification of a 21-Amino Acid Fragment with Neuroprotective Activity. *Mol. Neurobiol.* **2016**, *53*, 1165–1180. [CrossRef]
40. Rawat, V.; Wang, S.; Sima, J.; Bar, R.; Liraz, O.; Gundimeda, U.; Parekh, T.; Chan, J.; Johansson, J.O.; Tang, C.; et al. ApoE4 Alters ABCA1 Membrane Trafficking in Astrocytes. *J. Neurosci.* **2019**, *39*, 9611–9622. [CrossRef]
41. Rawat, V.; Banik, A.; Amaradhi, R.; Rojas, A.; Taval, S.; Nagy, T.; Dingledine, R.; Ganesh, T. Pharmacological antagonism of EP2 receptor does not modify basal cardiovascular and respiratory function, blood cell counts, and bone morphology in animal models. *Biomed. Pharmacother.* **2022**, *147*, 112646. [CrossRef]

42. Smith, S.M.; Min, J.; Ganesh, T.; Diebold, B.; Kawahara, T.; Zhu, Y.; McCoy, J.; Sun, A.; Snyder, J.P.; Fu, H.; et al. Ebselen and congeners inhibit NADPH oxidase 2-dependent superoxide generation by interrupting the binding of regulatory subunits. *Chem. Biol.* **2012**, *19*, 752–763. [CrossRef]
43. Zielonka, J.; Kalyanaraman, B. Hydroethidine- and MitoSOX-derived red fluorescence is not a reliable indicator of intracellular superoxide formation: Another inconvenient truth. *Free Radic. Biol. Med.* **2010**, *48*, 983–1001. [CrossRef] [PubMed]
44. Michalski, R.; Thiebaut, D.; Michałowski, B.; Ayhan, M.M.; Hardy, M.; Ouari, O.; Rostkowski, M.; Smulik-Izydorczyk, R.; Artelska, A.; Marcinek, A.; et al. Oxidation of ethidium-based probes by biological radicals: Mechanism, kinetics and implications for the detection of superoxide. *Sci. Rep.* **2020**, *10*, 18626. [CrossRef] [PubMed]
45. Roy, K.K.; Lu, J.; Doroshow, J.H. Effects of Iodonium Analogs on Nadph Oxidase 1 in Human Colon Cancer Cells. *Antioxidants* **2021**, *10*, 1757. [CrossRef] [PubMed]
46. Li, M.; Liu, Z.; Zhuan, L.; Wang, T.; Guo, S.; Wang, S.; Liu, J.; Ye, Z. Effects of apocynin on oxidative stress and expression of apoptosis-related genes in testes of diabetic rats. *Mol. Med. Rep.* **2013**, *7*, 47–52. [CrossRef] [PubMed]
47. Teleanu, D.M.; Niculescu, A.-G.; Lungu, I.I.; Radu, C.I.; Vladâcenco, O.; Roza, E.; Costăchescu, B.; Grumezescu, A.M.; Teleanu, R.I. An Overview of Oxidative Stress, Neuroinflammation, and Neurodegenerative Diseases. *Int. J. Mol. Sci.* **2022**, *23*, 5938. [CrossRef]
48. Barnham, K.J.; Masters, C.L.; Bush, A.I. Neurodegenerative diseases and oxidative stress. *Nat. Rev. Drug Discov.* **2004**, *3*, 205–214. [CrossRef]
49. Onose, G.; Anghelescu, A.; Blendea, D.; Ciobanu, V.; Daia, C.; Firan, F.C.; Oprea, M.; Spinu, A.; Popescu, C.; Ionescu, A.; et al. Cellular and Molecular Targets for Non-Invasive, Non-Pharmacological Therapeutic/Rehabilitative Interventions in Acute Ischemic Stroke. *Int. J. Mol. Sci.* **2022**, *23*, 907. [CrossRef]
50. Moghaddam, M.H.; Bayat, A.H.; Eskandari, N.; Abdollahifar, M.A.; Fotouhi, F.; Forouzannia, A.; Rafiei, R.; Hatari, S.; Seraj, A.; Shahidi, A.; et al. Elderberry diet ameliorates motor function and prevents oxidative stress-induced cell death in rat models of Huntington disease. *Brain Res.* **2021**, *1762*, 147444. [CrossRef]
51. Obrador, E.; Salvador, R.; Lopez-Blanch, R.; Jihad-Jebbar, A.; Valles, S.L.; Estrela, J.M. Oxidative Stress, Neuroinflammation and Mitochondria in the Pathophysiology of Amyotrophic Lateral Sclerosis. *Antioxidants* **2020**, *9*, 901. [CrossRef] [PubMed]
52. Solleiro-Villavicencio, H.; Rivas-Arancibia, S. Effect of Chronic Oxidative Stress on Neuroinflammatory Response Mediated by $CD4^+$T Cells in Neurodegenerative Diseases. *Front. Cell. Neurosci.* **2018**, *12*, 114. [CrossRef] [PubMed]

Disclaimer/Publisher's Note: The statements, opinions and data contained in all publications are solely those of the individual author(s) and contributor(s) and not of MDPI and/or the editor(s). MDPI and/or the editor(s) disclaim responsibility for any injury to people or property resulting from any ideas, methods, instructions or products referred to in the content.